Bull. Inst. Chem. Res., Kyoto Univ., Vol. 57, No. 1, 1979

Experimental Research on Penetration of Neutrons and Photons Produced in a Graphite Target Bombarded by 52-MeV Protons

Kazuo SHIN, Mitsuo YOSHIDA, Yoshitomo UWAMINO, Tomonori HYODO,* and Takashi NAKAMURA**

Received October 20, 1978

For the purpose to get necessary data for accelerator shielding and for transportation of secondary neutrons and gamma rays in a human body irradiated by high energy protons, penetration of neutrons and gamma rays produced in a graphite target by bombardment of 52-MeV protons was measured by a NE-213 organic liquid scintillator for iron, graphite, water and concrete barriers. Spectra and attenuation curves of neutrons and gamma rays penetrating the barriers are shown in this paper. Values of effective removal cross section for neutrons and effective attenuation coefficient for gamma rays are calculated from the attenuation curves.

KEY WORDS FM-cyclotron / Neutron attenuation / Gamma-ray attenuation / Accelerator Shielding / Neutron spectroscopy /

I. INTRODUCTION

Effective shielding for high energy neutrons and photons produced by high energy accelerators is necessary to maintain safety of people working with and living nearby them. Exact data of transportation of neutrons and photons through materials are necessary for the design study of the shielding.

Attenuation of neutrons produced by 80-MeV alpha-particle bombardment in iron and concrete was measured by Wadman,[1] using activation method. Transmission of neutrons and gamma rays from the ^{9}Be(d, n) reaction at 50 MeV through materials was measured by Meulders *et al.*[2] separating each other using time-of-flight method. There is no paper on the space-energy distribution of neutrons in energy over 15 MeV and associated gamma rays penetrating through materials. Systematic evaluation of cross sections and benchmark calculations have not been carried out for the neutrons in this energy region.

Spectra and yield of neutrons and photons from a thick graphite target bombarded by 52-MeV protons have been measured by the authors,[3] and the penetration of their neutrons and photons through graphite slabs was measured and compared with Monte Carlo calculation.

* 秦 和夫, 吉田光男, 上蓑義朋, 兵藤知典 : Department of Nuclear Engineering, Faculty of Engineering, Kyoto University, Kyoto.
** 中村尚司 : Institute for Nuclear Study, University of Tokyo, Tokyo.

In this paper, measurements of neutrons and gamma rays penetrating through graphite, water, concrete and iron will be described. The results will be shown in the form of the effective removal cross section for total neutrons ($\geq$2 MeV) and high energy group neutrons ($\geq$20 MeV), the effective attenuation coefficient for gamma rays ($\geq$3.0 MeV).

II. EXPERIMENTAL

II.1 Experimental Method

The experiments were carried out using 52-MeV protons accelerated by the FM-cyclotron of the Institute for Nuclear Study, University of Tokyo. The proton beam was taken out to the atmosphere through stainless steel foil of 0.15 mm in thickness. The protons bombarded a graphite target of 21.45 mm in thickness which is enough to stop the protons.

Slabs of graphite, water, ordinary concrete, and iron are placed 3 cm from the target as shown in Fig. 1. Dimension of the slabs and composition of materials are shown in Table I. The width and height may be enough for this experiment considering that neutron and photons produced in the target have very strong peak of the differential scattering cross section in the forward direction.[4]

Liquid organic scintillator NE-213 encapsulated in an aluminum can of 5.08 cm (2 in.) in diameter by 5.08 cm (2 in.) in length was used as a detector. The detector was placed in contact with the rear face of the slab. The block diagram of the detec-

Table I. Properties and Dimensions of Assemblies Used in the Experiment

Material	Elements (%wt)	Density (g/cm^3)	Dimensions Width × Height × Thickness (cm)
Graphite	C 100	1.68	90 × 54 × 21.5 〃 × 〃 × 43 〃 × 〃 × 64.5
Iron	Fe 99.99	7.86	50 × 52 × 20 〃 × 〃 × 40 〃 × 〃 × 60
Water	H_2O 100	1.0	80 × 55 × 60 〃 × 〃 × 100 〃 × 〃 × 160
Concrete	SiO_2 60.8 CaO 13.7 Al_2O_3 15.9 H_2O 3.6 Fe_2O_3 0.72 MgO 0.58 SO_3 0.48 Residue 4.3	2.3	75 × 60 × 46 〃 × 〃 × 69 〃 × 〃 × 115

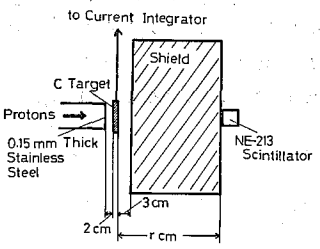

Fig. 1. Experimental arrangement. The thickness of the graphite target is 2.145 cm.

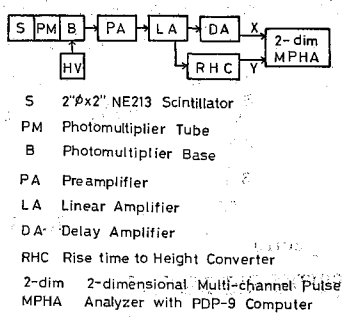

Fig. 2. Block diagram of detecting system.

ting system is shown in Fig. 2. Output pulses of the photomultiplier-tube-base circuit were sorted as neutron or photon pulses using rise-time-to-height converter (RHC), and an n-γ sorting program[5] and stored to a multi-channel pulse-height analyzer. The dynamic range of the RHC could not cover the energy region of neutrons (2—40 MeV), measurements were carried out deviding the region in two parts. The pulse height distributions of two parts were unfolded in series and obtained an energy spectrum. Calibration of the pulse height was done using 4.43-MeV gamma rays from an Am-Be neutron source and 1.17- and 1.33-MeV gamma rays from ^{60}Co.

To eliminate pile up of the output pulses of the detector, the proton beam intensity was maintained as low as possible. The beam intensity was measured by a current integrator connected with the graphite target.

II.2 Data Analysis

Unfolding of pulse-height distributions to energy spectra was carried out by FERDO code.[6] A light yield curve and a response function matrix are indispensable for the unfolding and reliability of the unfolding depends upon them. For the pulse-height distributions of neutrons obtained in this experiment, the curve must have the energy range up to 40 MeV. Only one curve published by Verbinski *et al.*[7] was available, and there was no response function for neutrons higher than 15 MeV.

In this study the curve and the response function were calculated with following procedure. A curve of pulse height *v. s.* proton energy was obtained as pulse height of the upper edge of pulse-height distributions of monoenergy neutrons of 3, 8, 9, 11, 12.5, and 15 MeV. The curve was extrapolated up to 45 MeV using Birk's formula.[8] The response functions for neutrons and gamma rays were obtained by Monte Carlo calculation.[9,10] It was known by Lockwood *et al.*[11] that at a high energy region the neutron response function had a bump which might be caused by the ^{12}C(n, p) reaction. Considering the form of neutron spectra in this experiment the bump was supposed to be small, and the reaction was calculated by the evaporation model. The energy of the most of gamma photons was less than 10 MeV, so the energy range of the response function for gamma rays was up to 10 MeV.

III. RESULTS AND DISCUSSION

III.1 Neutrons

The spectrum of source neutrons produced in the graphite target bombarded by 52-MeV protons is shown in Fig. 3. Neutron spectra penetrating the slabs are shown in Figs. 4 to 7. The spectra penetrating iron slabs have no significant difference in the form of spectra with the slab thickness as shown in Fig. 4. The relative slight increase of low energy neutrons with increase of graphite thickness is seen in the spectra shown

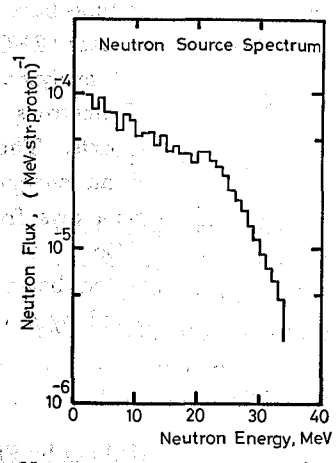

Fig. 3. Neutron source spectrum emitted at 0° from the graphite target of 2.145 cm in thickness.

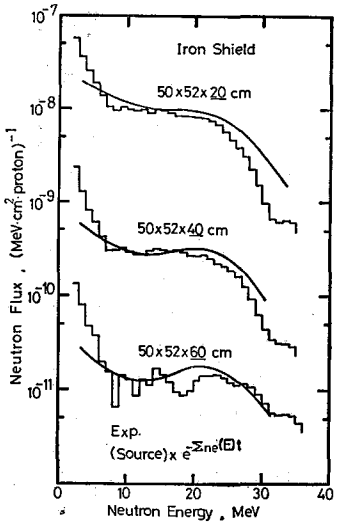

Fig. 4. Measured and estimated neutron spectra transmitted through iron slabs.

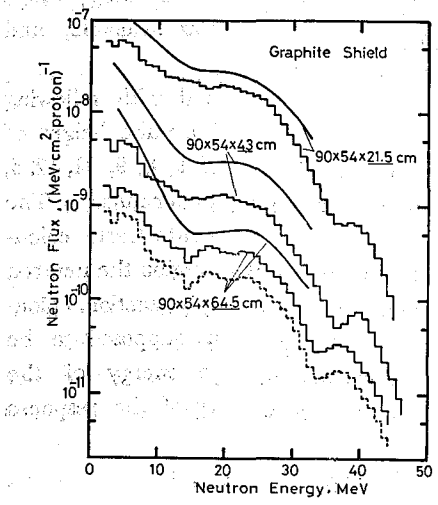

Fig. 5. Measured and estimated neutron spectra transmitted through graphite slabs.

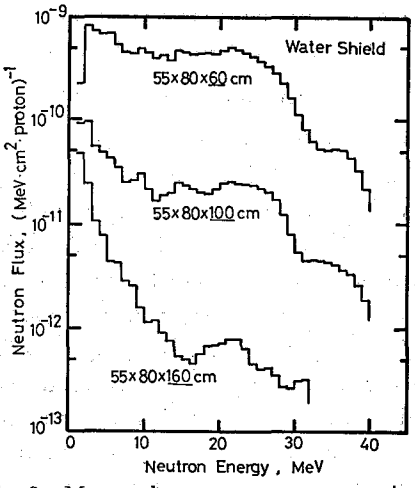

Fig. 6. Measured neutron spectra transmitted though concrete slabs.

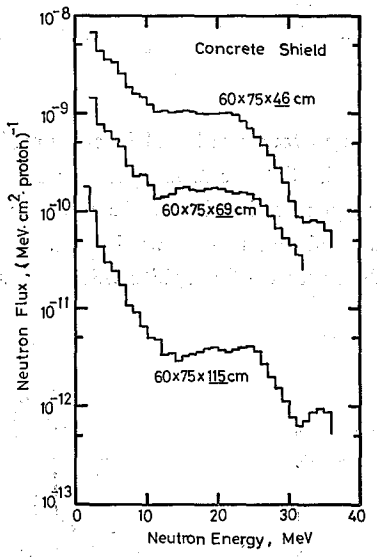

Fig. 7. Measured neutron spectra transmitted through water slabs.

in Fig. 5. The spectrum penetrating 64.5-cm thick graphite have deviation which might be caused by the error in the measurement of absolute value of the proton beam current, and the corrected spectrum is shown as dotted line. The spectra shown in Fig. 5 have neutrons over 40-MeV region, these neutrons may be produced in the stainless steel foil at the terminal of the beam duct. The neutron spectrum penetrating the concrete slab of 115 cm in thickness, shown in Fig. 7, have a characteristic form which has a valley at 12 MeV.

All of the spectra shown in Figs. 4 to 7 show increase of slow neutrons. This increase is larger for thicker slabs in the same material and water is the largest among the four materials used in this experiment. This increase starts at 7 MeV for iron and 11 to 12 MeV for the other materials. The cause may be that iron has large inelastic scattering cross section until lower than 10 MeV.

The calculated spectra shown in Figs. 4 and 5 were obtained by following formula,

$$N(E) = N_0(E)\, e^{-\Sigma_{ne}(E)t}$$

where $N_0(E)$ is a neutron spectrum emitted from the graphite target to the direction of the proton beam shown in Fig. 3, $\Sigma_{ne}(E)$ is nonelastic cross section for the neutron in energy E, t is thickness of the slab.

In the comparison of the calculated neutron attenuation to the experimental, they show in good agreement for the iron slabs in the energy region over 7 MeV and experimental spectra are larger than calculated below 7 MeV. They are in similar form in high energy region for the graphite slabs and the spectra obtained by experiment are smaller than calculated. This trend becomes larger with increasing the slab thickness and in lower energy region in the same thickness.

These phenomena may be understandable as following. Neutrons in high energy region attenuate in iron slabs mainly by nonelastic reaction and neutron pile up in low energy region may occur by inelastic scattering and (n, 2n) reaction at high energy

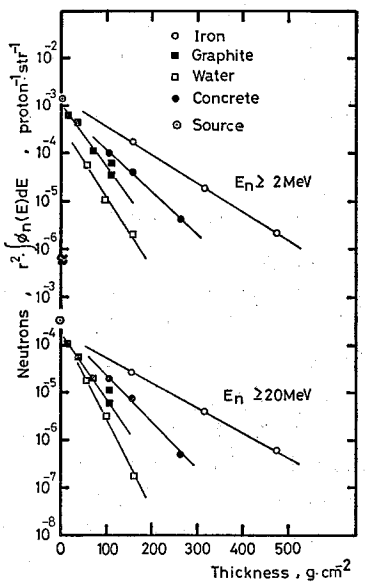

Fig. 8. Attenuation of total neutrons (E_n=2 MeV) and high energy group neutrons (E_n=20 MeV) with shield thickness.

region. In graphite slabs elastic scattering affect the attenuation of neutrons and it is predominant in low energy region.

Attenuation curves of total neutrons (≧2.2 MeV) and high energy group neutrons (≧20 MeV) are shown in Fig. 8. The point for graphite of 64.5 cm in thickness deviates from the curve. Correction of the spectrum of 64.5-cm graphite in Fig. 5 was made to fit the point on the curve.

The macroscopic effective removal cross section, inverse of the attenuation length, was calculated from these attenuation curves and shown in Table II. Comparing these values for both neutron group, the values for high energy group neutrons are smaller than those of total neutrons excluding graphite. The values for graphite are nearly equal for both energy group of neutrons. The cause can not discuss here because the thickness of graphite slabs were not enough for the measurement of attenuation omitting the barrier of 64.5 cm. Value of the removal cross section for 12.5 MeV, which

Table II. Macroscopic Removal Cross Section for Iron, Graphite, Water, and Concrete

Material	Effective Macroscopic Removal Cross Section (cm^2/g)		Macroscopic Removal Cross Section (cm^2/g)
	High Energy Group Neutrons ($E_n \geq 20$ MeV)	Total Neutrons ($E_n \geq 2$ MeV)	Reference Data*
Iron	1.18×10^{-2}	1.39×10^{-2}	1.703×10^{-2}
Graphite	3.01×10^{-2}	3.10×10^{-2}	4.64×10^{-2}
Water	4.44×10^{-2}	3.16×10^{-2}	8.40×10^{-2}
Concrete	2.37×10^{-2}	2.04×10^{-2}	2.23×10^{-2}**

* These data of removal cross section were cited from Ref. 12

** Aluminum datum was used as that for concrete.

is nearby the average of total neutrons (12.9 MeV), is shown in Table II. There are no removal cross section for concrete, the value for aluminum is shown as a reference datum. The values obtained in this study are smaller than the values for 12.5 MeV. The cause may be that the former is the effective value for large energy region.

III.2 Photons

The spectrum of source gamma rays produced in the graphite target bombarded by 52-MeV protons is shown in Fig. 9. Gamma-ray spectra penetrating through iron, graphite, water and concrete are shown in Figs. 10 to 13. The large peak of 4.43 MeV in the source spectrum attenuates and distinct peak is seen at 7 MeV in the spectrum for iron of 60 cm in thickness as shown in Fig. 10. This peak may be neutron capture gamma rays of iron. The spectrum for graphite shown in Fig. 11 maintains the peak of 4.43 MeV up to 64.5 cm. The spectrum of dotted line shows the corrected spectrum for the 64.5-cm graphite slab. All of the spectra shown in Fig. 11 are in similar form. This phenomenon shows that most of the penetrating gamma rays through graphite slabs come from the target and the yield of secondary gamma rays by neutrons in the graphite slabs is not large.

Gamma-ray spectra penetrating through water slabs (Fig. 12) show that effect of the distinct peak at 4.43 MeV from the source gamma rays gradually vanishes and peaks of gamma rays from $^{1}H(n, \gamma)^{2}H$ and $^{16}O(n, n\gamma)^{16}O$ reactions become distinct as increasing the slab thickness. For the concrete slabs, spectra of Fig. 13 show that the peak of source gamma rays attenuate and the other small peaks are seen and they may be capture gamma rays of Si, Fe, H, *etc.*

Attenuation of 4.43-MeV gamma rays in the graphite and water slabs is shown in

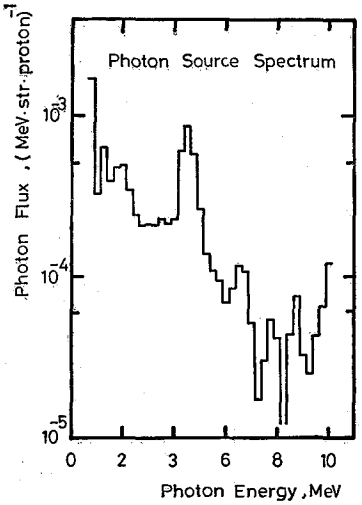

Fig. 9. Photon spectrum emitted at 0° from the graphite target of 2.145cm in thickness.

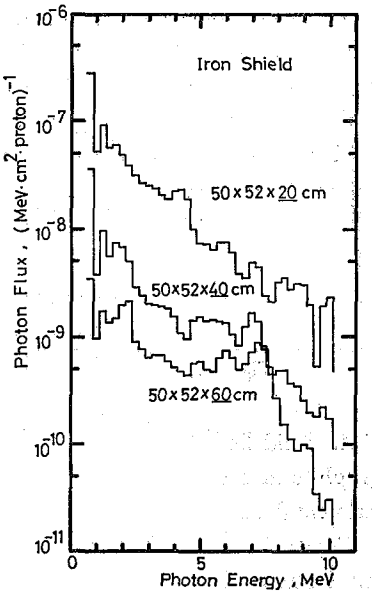

Fig. 10. Measured photon spectra transmitted through iron slabs.

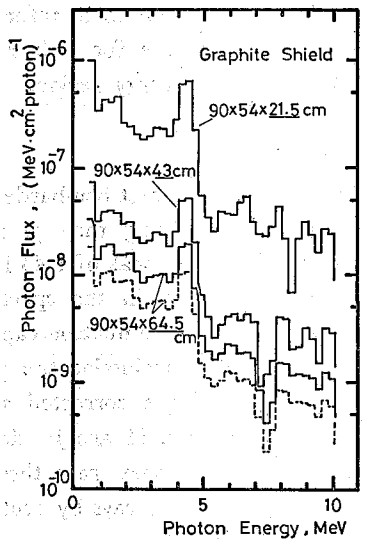

Fig. 11. Measured photon spectra transmitted through graphite slabs. The dotted line shows corrected spectrum for 64.5-cm thickness.

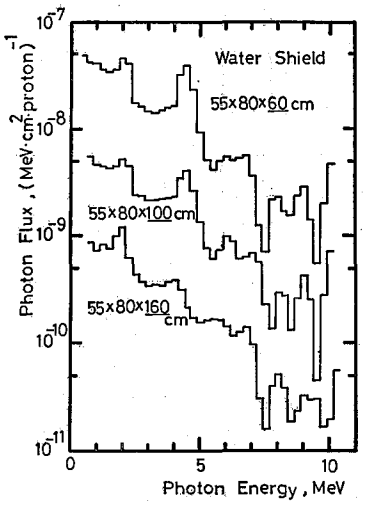

Fig. 12. Measured photon spectra transmitted through water slabs.

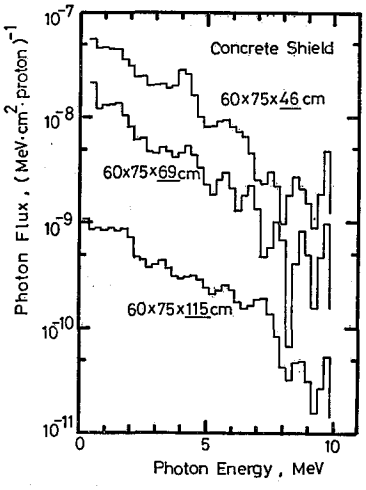

Fig. 13. Measured photon spectra transmitted through concrete slabs.

Fig. 14. Solid line in the figure shows $\exp(-\mu t)$, where μ is the attenuation coefficient of graphite and water for 4.43-MeV gamma rays and t is the thickness of slabs. The experimental values are in good fit for the exponential lines excluding graphite of 64.5 cm. Figure 15 shows the attenuation of total photons integrated over 0.3 MeV. The effective attenuation coefficient, inverse of the mean free path, was obtained from the figure for each material and shown in Table III. Values of the attenuation coefficient for 3.16 MeV, which is mean energy of source gamma rays, are shown in this table.

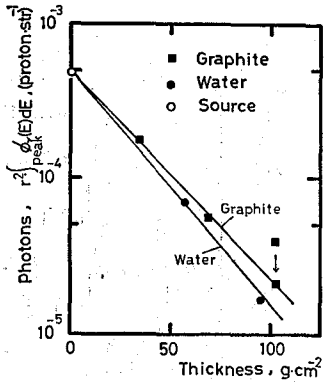

Fig. 14. Attenuation of measured photon flux at 4.43-MeV peak. Solid lines show attenuation with the linear attenuation coefficients of 4.43-MeV gamma rays.

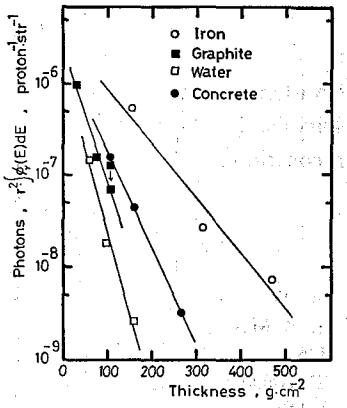

Fig. 15. Attenuation of integrated photon flux above 0.3 MeV with slab thickness.

Table III. Photon Attenuation Coefficients of Iron, Water, Graphite and Concrete Assemblies

Material	Attenuation Coefficients (cm^2/g)	
	Experimental*	Other Reference Data**
Iron	7.11×10^{-3}	3.57×10^{-2}
Water	2.02×10^{-2}	3.88×10^{-2}
Graphite	3.68×10^{-2}	3.49×10^{-2}
Concrete	1.42×10^{-2}	3.58×10^{-2}

* Effective attenuation coefficient for gamma rays over 0.3 MeV in energy.

** These attenuation coefficients were calculated from the data in Ref. 13.

Comparing both values, for the same material, graphite shows good agreement and the experimental values are smaller than values of the attenuation coefficient for the other materials. Secondary gamma rays affect the emerging gamma rays from the slabs excluding graphite.

IV. CONCLUSION

Spectra of neutrons and gamma rays penetrating through iron, graphite, water and concrete were obtained. These neutrons and gamma rays were measured single NE-213 scintillator at the same time sorting the output pulses of the scintillator. Attenuation curves for the neutrons and the gamma rays integrated these spectra are shown. Values of the effective removal cross section for neutrons and the effective attenuation coefficient for gamma rays were obtained from the attenuation curves. These data will be helpful for design study of accelerator shielding, and for estimation of the distribution of secondary neutrons and gamma rays in a human body irradiated by high energy protons.

ACKNOWLEDGMENT

The authors wish to express their thanks to the Cyclotron Machine group of Low Energy Division for the FM-cyclotron operation, to Messrs. K. Takaku and K. Omata for their contribution, at Institute for Nuclear Study, University of Tokyo.

REFERENCES

(1) W. W. Wadman, III, *Nucl. Sci. Eng.*, **35**, 220 (1969).
(2) J. P. Meulders, P. Leleux, P. C. Macq, C. Pirart, and G. Valenduc, *Nucl. Instr. Methods*, **126**, 81 (1975).
(3) T. Nakamura, M. Yoshida, and K. Shin, *Nucl. Instr. Methods*, **151**, 493 (1978).
(4) K. Shin, Y. Uwamino, M. Yoshida, and T. Hyodo, preparing for the publication.
(5) T. Nakamura, K. Omata. K. Shin, M. Yoshida, Y. Uwamino, and K. Hayashi, *Genshikaku Kenkyu*, **22**, No. 6, 1 (1978), in Japanese.
(6) W. R. Burrus and V. V. Verbinski, "Recent Development in the Proton-Recoil Scintillation Neutron Spectrometer", AND-SD-2, American Nuclear Society, (1964), pp. 148-188.
(7) V. V. Verbinski, W. R. Burrus, T. A. Love, W. Zobel, and N. W. Hill, *Nucl. Instr. Methods*, **65**, 8 (1968).
(8) V. V. Verbinski, J. C. Courtney, W. R. Burrus, and T. A. Love, "The Response of Some Organic Scintillators to Fast Neutrons", ANS-SD-2, American Nuclear Society, (1964), pp. 189-231.
(9) K. Shin, H. Tokumaru, M. Yoshida, Y. Uwamino, and T. Hyodo, preparing for the publication.
(10) K. Shin, Y. Hayashida, and T. Hyodo, Preparing for the publication.
(11) J. A. Lockwood, C. Chen, L. A. Friling, D. Swartz, R. N. St. Onge, A. Galonsky, and R. R. Doering, *Nucl. Instr. Methods*, **138**, 353 (1976).
(12) J. Butler and A. F. Avery, "Removal-Diffusion Theory" in "Engineering Compendium on Radiation Shielding", Vol. I, R. G. Jaeger, ed., Springer-Verlag, Berlin, (1968), pp. 273-301.
(13) J. H. Hubbell, "Photon Cross Sections, Attenuation Coefficients, and Energy Absorption Coefficients from 10 keV to 100 GeV", NSRDS-NBS 29, United States Department of Commerce, (1969).